The contribution of boreal spring South Pacific atmospheric variability to the El Niño occurrence

2 authors:

Qingye Min
Fudan University
5 PUBLICATIONS **146** CITATIONS

SEE PROFILE

Renhe Zhang
Fudan University
199 PUBLICATIONS **5,686** CITATIONS

SEE PROFILE

Some of the authors of this publication are also working on these related projects:

Project   Year-to-year variability of surface air temperature over China in winter: CHINA SURFACE AIR TEMPERATURE View project

Project   ENSO, global warming View project

The Contribution of Boreal Spring South Pacific Atmospheric Variability to El Niño Occurrence

QINGYE MIN AND RENHE ZHANG

Department of Atmospheric and Oceanic Sciences and Institute of Atmospheric Sciences, Fudan University, and CMA-FDU Joint Laboratory of Marine Meteorology, Shanghai, and Innovation Center of Ocean and Atmosphere System, Zhuhai Fudan Innovation Research Institute, Zhuhai, China

ABSTRACT

Despite the fact that great efforts have been made to improve the prediction of El Niño events, it remains challenging because of limited understanding of El Niño and its precursors. This research focuses on the influence of South Pacific atmospheric variability on the development of the sea surface temperature anomaly (SSTA) in the tropical Pacific. It is found that as early as in the boreal spring of El Niño years, the sea level pressure anomaly (SLPA) shows a configuration characterized by two significant negative anomaly centers in the north and a positive anomaly center in the south between the subtropics and high latitudes in South Pacific. Such an anomalous SLPA pattern becomes stronger in the following late boreal spring and summer associated with the strengthening of westerly anomalies in the tropical Pacific, weakening the southeasterly trade winds and promoting the warming of tropical eastern Pacific, which is conducive to the development of El Niño events. It is demonstrated that the SLPA pattern in boreal spring revealed in this study is closely associated with boreal summer South Pacific Oscillation (SPO) and South Pacific meridional mode (SPMM). As a precursor in boreal spring, the prediction skill of the South Pacific SLPA in boreal spring for the SSTA in the eastern equatorial Pacific is better than that of the SPMM. This study is helpful to deepen our understanding of the contribution of South Pacific extratropical atmospheric variability to El Niño occurrence.

1. Introduction

El Niño is a phenomenon with significant impacts on the climate of many regions over the world and is of great significance to the short-term climate prediction. For El Niño occurrence, previous studies have found many important precursors, such as the westerly burst (e.g., Fedorov 2002) and warm water volume (e.g., Meinen and McPhaden 2000; McPhaden 2012) in the tropical Pacific, the North and South Pacific meridional modes (e.g., Chiang and Vimont 2004; Chang et al. 2007; Zhang et al. 2014; Min et al. 2017), and North and South Pacific Oscillations (e.g., Walker and Bliss 1932; Linkin and Nigam 2008; You and Furtado 2017). It has been recognized that there are different types of El Niños that occur in the tropical Pacific (Wang and Weisberg 2000; Trenberth and Stepaniak 2001), and some studies divided El Niños into two types, the central Pacific and eastern Pacific El Niños (Ashok et al. 2007; Kao and Yu 2009; Kug et al. 2009). More and more studies have

focused on investigating different precursors for El Niño diversity in recent years (e.g., Min et al. 2017; You and Furtado 2017, 2018).

In the past two decades, many studies have demonstrated that the evolution and amplitude of El Niño are closely associated with the extratropical atmospheric variability (e.g., Pierce et al. 2000; Sun et al. 2004; Zheng et al. 2014; Min et al. 2015; Su et al. 2018). Zhang et al. (2001) showed that El Niño is significantly related to the meridional wind stress over subtropical central Pacific as early as half a year prior to El Niño occurrence. A few investigators have also proposed a physical relationship between the northern Pacific atmospheric internal variability and El Niño in boreal winter (Vimont et al. 2001, 2003a,b; Alexander et al. 2010; Yu and Kim 2011). Vimont et al. (2001) first proposed the seasonal footprint mechanism to explain the relationship between the northern Pacific atmospheric internal variability and El Niño evolution in boreal winter. Vimont et al. (2003a) suggested that during boreal winter season, intrinsic atmospheric variability in North Pacific midlatitudes has a spatial structure that closely resembles the North

Corresponding author: Renhe Zhang, rhzhang@fudan.edu.cn

Pacific oscillation (NPO) (Walker and Bliss 1932; Rogers 1981) and imparts a sea surface temperature (SST) "footprint" onto the ocean via changing the net surface heat flux. This footprint can persist into the late boreal spring and summer. The subtropical portion of the SST footprint, in turn, forces a pattern of atmospheric circulation anomalies including zonal wind stress anomalies around the equator. Finally, the coupled tropical atmosphere–ocean system responds to the summer zonal wind stress anomalies through coupled dynamics, producing an equatorially symmetric, ENSO-like variability. The anomalous circulation associated with the southern pole of NPO can also effectively modulate the intensity of the trade winds outside the equator and then change the ocean heat content in central Pacific Ocean (Anderson et al. 2013; Anderson and Perez 2015), and finally trigger El Niño events. Moreover, the North Pacific meridional mode (NPMM), which is a low-frequency atmosphere–ocean coupled variability first discussed by Chiang and Vimont (2004), is found to be independent of ENSO, and has a robust relationship with ENSO in the multimodel ensemble retrospective forecasts (e.g., Larson and Kirtman 2014). Both NPO and NPMM are important precursors for El Niño events (Chang et al. 2007). However, it is still controversial whether NPO or NPMM is more conducive to the occurrence and development of a specific type of El Niño events (e.g., Yu et al. 2010; Yu and Kim 2011; Vimont et al. 2014; Ding et al. 2015; Di Lorenzo et al. 2015; Ding et al. 2017a).

Compared to the impact of North Pacific precursors, the influence of South Pacific precursors on the evolution of El Niño is relatively lacking. Zhang et al. (2001) found that the meridional wind stress from extra-equatorial eastern South Pacific converges with that from extra-equatorial eastern North Pacific in about half a year before El Niño onset, which is favorable for El Niño occurrence (Zhang and Zhao 2001). McGregor et al. (2009a,b) indicated that the extra-equatorial wind stress in South Pacific can affect the thermocline depth in the tropical Pacific, and is of great significance for the extended range forecast of El Niño. Ding et al. (2015) argued that a quadrupole sea surface temperature anomaly (SSTA) caused by the atmospheric variations in the middle latitudes of the South Pacific may affect the development and evolution of El Niño. They found a significant correlation of El Niño with the Pacific–South America (PSA) pattern prior to about 10–12 months. Their analysis showed that PSA and NPO have the same effect on the initiation of El Niño, both of which have significant influence on El Niño events in later boreal winter. Ding et al. (2017b) also investigated the relationship between the evolution of El Niño and the subtropical sea level pressure anomaly (SLPA) in the South and North Pacific prior to the

occurrence of El Niño events. They found that the synergistic effect of both the North and South Pacific SLPA could effectively affect the development of subsequent El Niño events. Although the source of the South Pacific meridional mode (SPMM) is not clear, Zhang et al. (2014) and Min et al. (2017) pointed out the importance of SPMM in the development of eastern Pacific El Niño events. You and Furtado (2017) pointed out that in boreal summer, the positive phase of the first empirical orthogonal function (EOF) mode of South Pacific SLPA (10°–45°S, 160°E–70°W), the so-called South Pacific Oscillation (SPO), is of great significance for the prediction of different type of El Niño events. They believed that the SPO also plays an important role in the formation and development of SPMM, and further discussed the synergistic effect of the NPMM and SPMM as precursors in El Niño prediction (You and Furtado 2018, 2019).

Although the influence of North Pacific precursors on the development of two types of El Niño has been reported by previous research work, the influence of South Pacific precursors remains unclear. As mentioned above, there is no consistent conclusion for the impact of the Southern Hemisphere atmospheric variability on the occurrence of El Niño. Previous studies have emphasized the role of different types of atmospheric circulation anomalies, such as the PSA and the so-called SPO on El Niño, but the relative role of these factors in the occurrence of El Niño is not clear. At present, the relationship between the atmospheric variability in the South Pacific and El Niño is still an open research issue. In this study, we will focus on the influence of boreal spring South Pacific atmospheric variability on the occurrence of conventional El Niño events, which has not been fully revealed. The remainder of this paper is organized as follows: data and analysis methods are described in section 2, results are presented in section 3, and a summary and discussion are given in section 4.

2. Data and methods

Monthly mean atmospheric fields (SLP, zonal component of momentum flux, SST) from 1948 to 2018 are from the National Centers for Environmental Prediction–National Center for Atmospheric Research (NCEP–NCAR) Reanalysis-1 product (NCEP/NCAR R1; Kalnay et al. 1996). The SST data are the skin temperature data from https://psl.noaa.gov/data/gridded/data.ncep.reanalysis.derived.surfaceflux.html. Monthly anomalies of all variables are derived by subtracting the monthly climatology in 1948–2018. Linear regression, composite, empirical orthogonal function (EOF), and maximum covariance analysis (MCA; Bretherton et al. 1992) are the main statistical methods used in this study. The two-tailed Student's

t test is applied to check the significance of correlation and regression coefficients. All data are linearly detrended before conducting analyses. The SPMM index used in the study is the same as that used in You and Furtado (2018), which is the leading MCA mode (MCA-1) of the cross-covariance matrix between SST and 10-m wind anomalies in the subtropical South Pacific (35°–10°S, 180°–70°W). The contemporaneous cold tongue index (Deser and Wallace 1990) is used to remove the local internal variability.

To understand the physical mechanisms responsible for the influence of extratropical precursor on the occurrence of El Niño, the mixed layer heat budget is diagnosed. The mixed layer temperature tendency equation can be written as

$$\frac{\partial T'}{\partial t} = -(\mathbf{V}' \cdot \nabla \overline{T} + \overline{\mathbf{V}} \cdot \nabla T') - (\mathbf{V}' \cdot \nabla T') + \frac{\mathbf{Q}'_{\text{net}}}{\rho C_p H} + R, \quad (1)$$

where $\mathbf{V} = (u, v, w)$ represents the 3D ocean current, $\nabla = [(\partial/\partial x), (\partial/\partial y), (\partial/\partial z)]$ denotes the 3D gradient operator, a prime ($'$) represents the variable anomaly, an overbar ($^-$) represents the variable's climatological annual cycle, $-(\mathbf{V}' \cdot \nabla \overline{T} + \overline{\mathbf{V}} \cdot \nabla T')$ is the sum of linear temperature advection terms, $-(\mathbf{V}' \cdot \nabla T')$ denotes 3D nonlinear anomalous temperature advection terms, $\mathbf{Q}_{\text{net}}$ represents the net heat flux at the ocean surface, R represents the residual term, $\rho = 10^3 \text{ kg m}^{-3}$ represents the density of water, $C_p = 4000 \text{ J kg}^{-1} \text{ K}^{-1}$ represents the specific heat of water, and H denotes the climatological mixed layer depth. The mixed layer depth data in 1948–2010 are from the French Research Institute for Exploration of the Sea (de Boyer Montégut et al. 2004), which are used to determine the climatological mixed layer depth. Anomalies of all these variables are derived by subtracting their long-term climatology (1948–2010). The heat budget terms are calculated based on the Simple Ocean Data Assimilation 2.2.4 (SODA; Carton and Giese 2008) and NCEP–NCAR R1 heat flux datasets (Kalnay et al. 1996).

ENSO events are defined based on a threshold of +0.5°C for the 3-month running mean of NCEP–NCAR R1 SST anomalies in the Niño-3.4 region (5°N–5°S, 170°–120°W), and an El Niño year is defined when the threshold is met for a minimum of 5 consecutive overlapping seasons. According to such criteria, there are 18 El Niño years during 1948–2018, occurring in 1957, 1963, 1965, 1968, 1969, 1972, 1976, 1977, 1982, 1986, 1987, 1991, 1994, 1997, 2002, 2004, 2009, and 2015.

It is worth noting that here we use two sets of reanalysis data, NCEP–NCAR R1 (Kalnay et al. 1996) and ERA-20C (Poli et al. 2013), for checking the
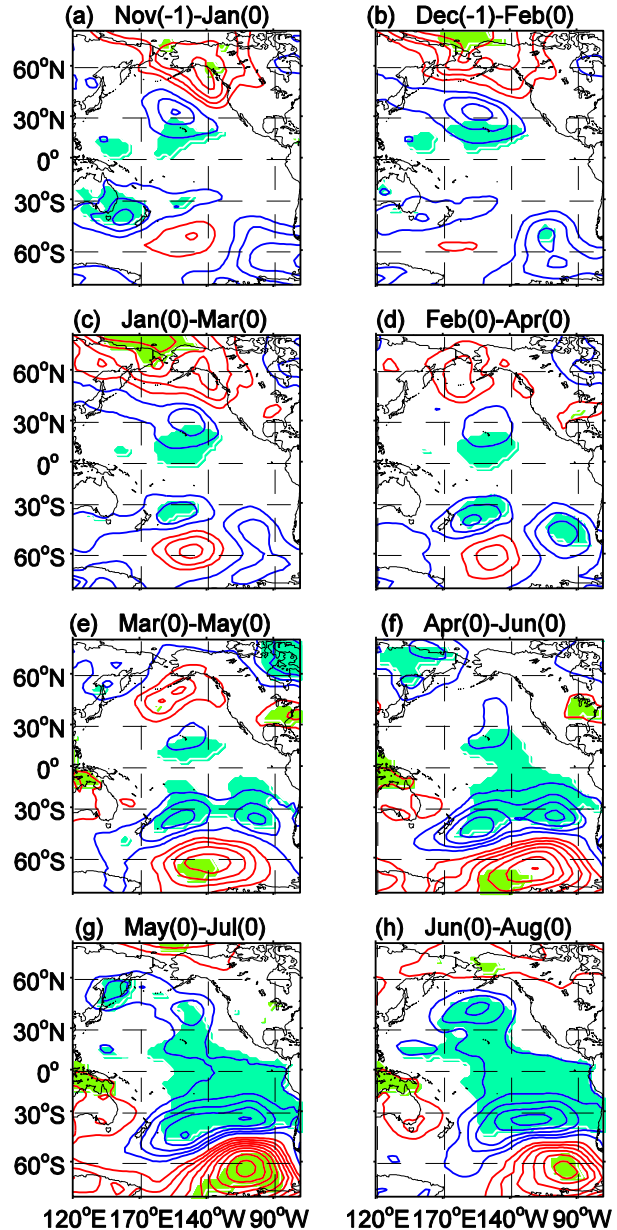

FIG. 1. Composites of sea level pressure anomaly (SLPA) in El Niño years (contours, with intervals of 0.4 hPa). Blue and red lines are negative and positive values, respectively. The green and orange shading are negative and positive SLPA, respectively, exceeding the 95% significance level.

robustness of our analyses. Because the results are nearly the same, we only give the results from NCEP–NCAR R1 data in section 3. Additionally, Zhu et al. (2012) pointed out that there exist significant uncertainties in the thermal states in different ocean data assimilations. In our present study the data from the Global Ocean Data Assimilation System (GODAS; Saha et al. 2006) from 1980 to 2018 are also used to check
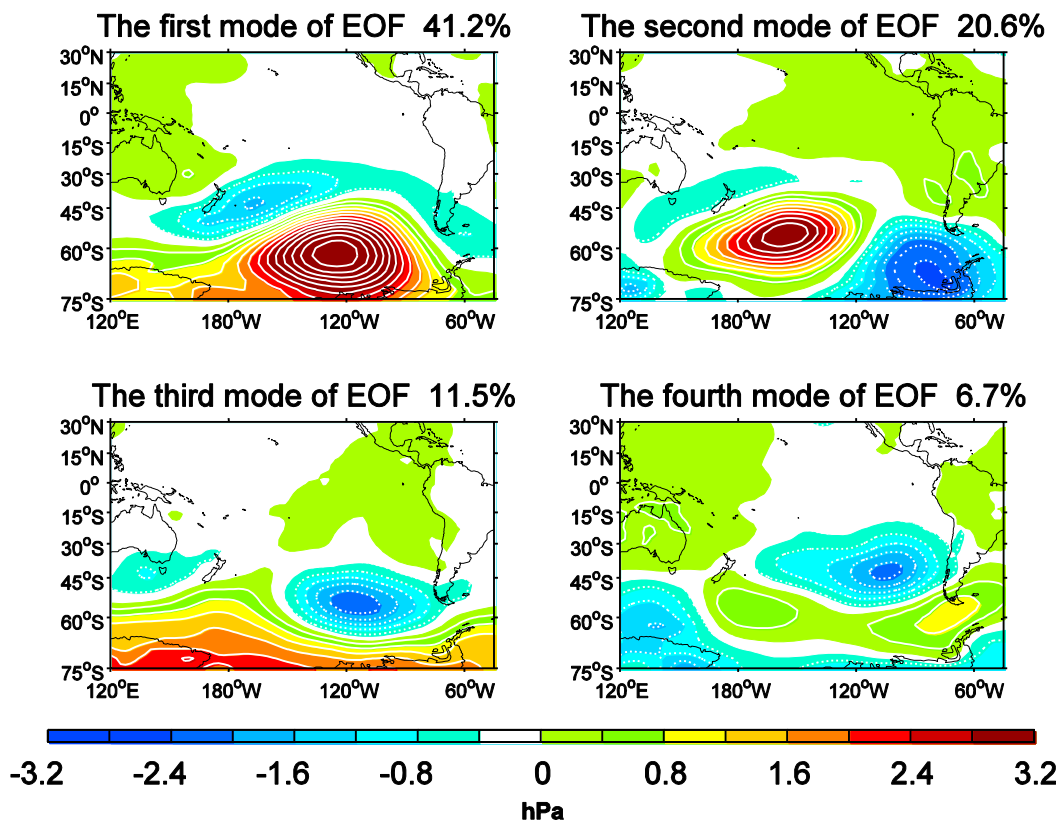
FIG. 2. Regressed normalized SLPA field against PCs of first four EOF modes over the South Pacific in the region 15°–75°S, 160°E–70°W in boreal spring (MAM) for the period 1948–2018. The solid and dashed lines indicate positive and negative anomalies, respectively.

the results from the SODA data. The results from the GODAS data are quite similar to those from the SODA data.

3. Results

a. The South Pacific precursor and its influence on El Niño

Figure 1 presents the composite of SLPA in El Niño years. In the previous boreal winter of El Niño years, there is an obvious negative SLPA center (Figs. 1a,b) in the subtropical region of the North Pacific Ocean, which is the southern pole of NPO and has been studied in detail by Vimont et al. (2001, 2003a,b) for its influence on the development of El Niño. However, such signal is getting weaker. We can find that at the beginning of El Niño years, the SLPA field in the Southern Hemisphere presents a distribution pattern of two negative anomaly centers at around 40°S, 165°W and 40°S, 110°W in the north, and one positive anomaly center at around 65°S, 140°W in the south (Figs. 1c,d). Such SLPA pattern resembles the PSA precursor pattern preceding El Niños

identified by Ding et al. (2015). During the boreal spring (March–May) of El Niño years, there are more significant SLPA in the South Pacific than in the North Pacific (Fig. 1e). In the following boreal late spring and summer, the negative SLPA centers at around 40°S, 165°W and 40°S, 110°W in the north gradually strengthened and merged into one negative anomaly center (Figs. 1f–h), which is a typical SLPA pattern of the SPO (You and Furtado 2017). It can be seen that the significant signal associated with the SPO can appear in the South Pacific in boreal spring of El Niño years, which is almost one season earlier than the appearance of the SPO in boreal summer as pointed out by You and Furtado (2017). Meanwhile, it seems that the signals of SLPA in the South Pacific are much stronger than those in the North Pacific prior to El Niño events from boreal spring to summer of El Niño years, indicating possibly a more important role of preceding South Pacific SLPA signals in the occurrence of El Niño events.

The SLPA associated with SPO appears in boreal spring of El Niño years. Nevertheless, is this SLPA pattern an independent EOF mode as suggested by You and Furtado (2017)? Here we perform an EOF analysis
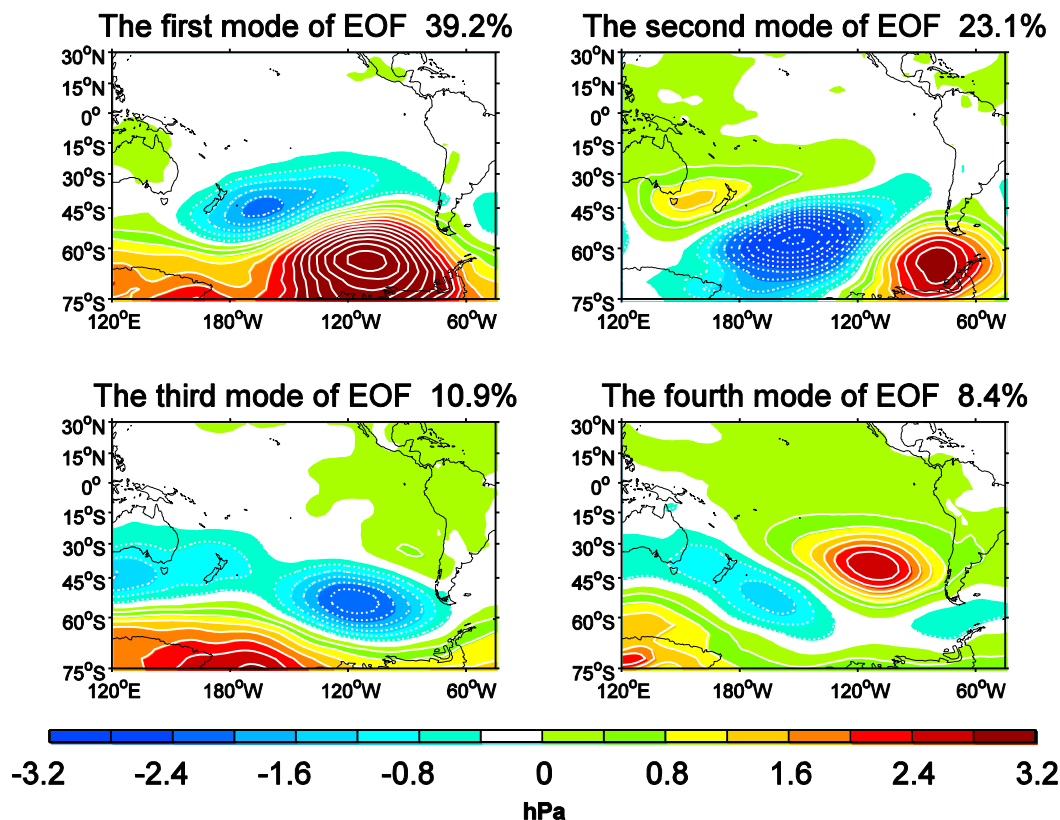
FIG. 3. As in Fig. 2, but in boreal summer.

for the South Pacific SLPA (15°–75°S, 160°E–70°W) in boreal spring (Fig. 2). Although the four leading independent EOF modes account for about 80% of the total variance, none of them can fully reflect the composite South Pacific SLPA during boreal spring of El Niño years. It is not difficult to find that the position of the SLPA centers in the first and fourth modes is similar to that in Fig. 1e. Here we calculate the spatial correlation coefficients between the four leading EOF modes and the South Pacific (15°–75°S, 160°E–70°W) SLPA in boreal spring, which are 0.90, 0.21, 0.09, and 0.43, respectively. The spatial correlation coefficients between the SLPA field and the first and fourth EOF mode shown in Fig. 2 are significantly higher than those of other two EOF modes. Further, we also perform the EOF analysis for the South Pacific (15°–75°S, 160°E–70°W) SLPA during boreal summer (Fig. 3). The results of the four leading EOF modes accounting for about 80% of the total variance are very similar to those in Fig. 2. It means that the SLPA associated with SPO appeared in boreal spring of El Niño years is not an independent EOF mode, but related to two EOF modes (the first and fourth EOF modes), both of which may be related with El Niño occurrence.

How can the South Pacific (15°–75°S, 160°E–70°W) SLPA in boreal spring affect the development of SSTA in equatorial Pacific? Here we use the principal component time series of the first EOF mode for the South Pacific (15°–75°S, 160°E–70°W) SLPA during boreal spring (PC1) to regress the SLP, the zonal wind stress, and the SST anomalies over Pacific in boreal spring, the following boreal summer, autumn, and winter. The results are shown in Fig. 4. It can be seen that this EOF mode is associated with the development of SPO around the region 20°–40°S, 160°–100°W in boreal summer. And at the same time, it also contributes to the enhancement of the westerly wind anomaly near the date line to some extent. The westerly wind anomaly can activate the eastward propagation of Kelvin waves, and contribute to the increase of the eastern equatorial Pacific SST in the following boreal autumn and winter. However, although this EOF mode captures 41.2% of the total variance, its impact on SSTA in the equatorial Pacific is limited. The highest SSTA regressed in the equatorial eastern Pacific in boreal autumn and winter can only reach 0.4°C.

Considering the importance of the fourth EOF mode in El Niño occurrence, we use the sum of the PC1 and the fourth EOF principal component time series (PC4)
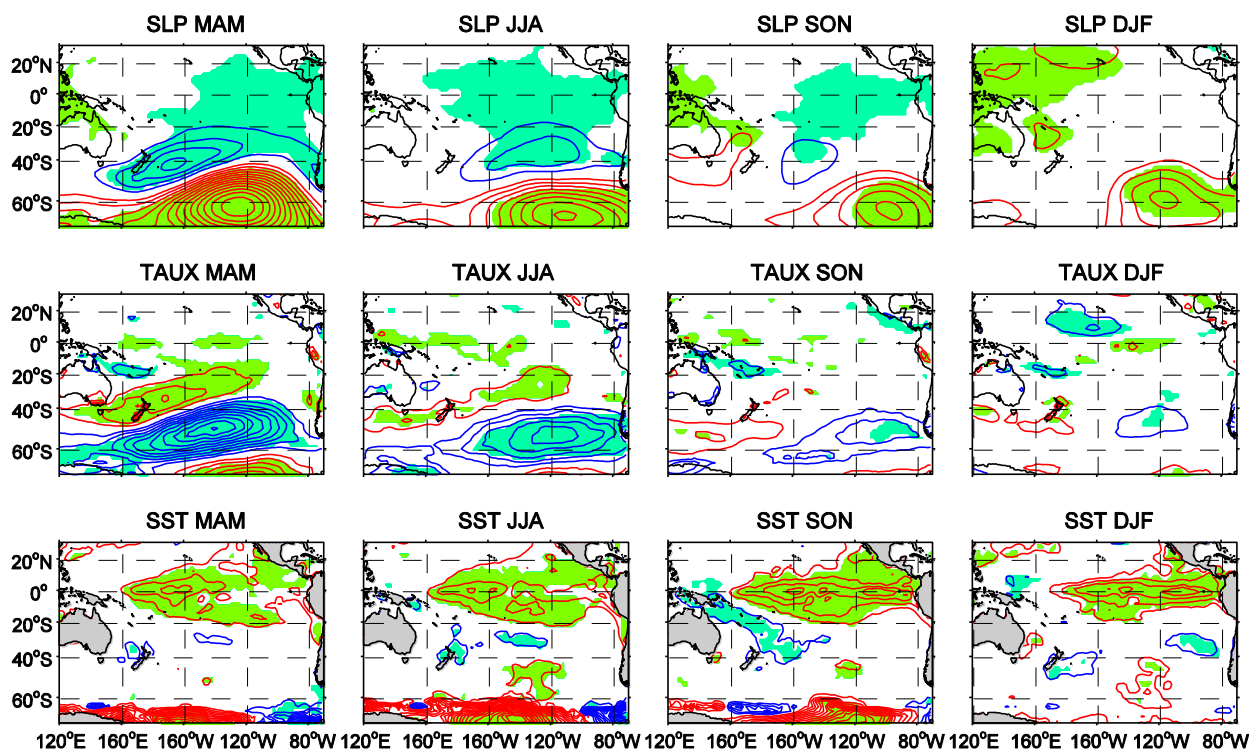
FIG. 4. Regressed anomalies of (top) SLP (units: hPa; contours with 0.4-hPa interval), (middle) zonal wind stress (units: N m^{-2}; contours with 5×10^{-3} N m^{-2} interval), and (bottom) SST (units: °C; contours with 0.1°C interval) from boreal spring (MAM) to winter (DJF) against the PC of the first EOF mode for normalized MAM SLPA over South Pacific in the region 15°–75°S, 160°E–70°W for the period 1948–2018. Blue and red lines are negative and positive values, respectively. The shaded areas in all panels are significant above the 95% confidence level.

to regress the SLP, zonal wind stress, and SST anomalies over Pacific in boreal spring, and the following boreal summer, autumn, and winter. As shown in Fig. 5, the regressed South Pacific SLPA in boreal spring is very similar to that of the composite results (Fig. 1e). When the PC4 is additionally incorporated (Fig. 5), the SLPA pattern of two negative anomaly centers at around 40°S, 165°W and 40°S, 110°W in the north and the positive anomaly center at around 65°S, 140°W in the south in boreal spring is more significant. The westerly wind anomaly becomes much stronger, which can excite an eastward Kelvin wave and results in the SST warming in equatorial Pacific, especially in the eastern equatorial Pacific. The SST warming is more significant during boreal autumn and winter of El Niño years, and the maximum SSTA can exceed 0.7°C, which is much larger than the 0.4°C when only the PC1 is considered (Fig. 4). The SLPA in boreal spring develops into a typical SPO pattern in the following boreal summer. In response to the anomalous southwesterlies associated with the SPO, the southeasterly trade winds become weaker and subsequently weaken the upward latent heat flux, which warm the local ocean and lead to a negative wind–

evaporation–SST feedback there (Xie and Philander 1994). As a result, the signal of stronger westerly wind anomaly can gradually propagate to the equator from the extratropical region.

Generally, although the fourth EOF mode of South Pacific (15°–75°S, 160°E–70°W) SLPA in boreal spring only captures 6.7% of the total variance, it serves as an important precursor for both the evolution of SPO in the southeast Pacific during boreal summer and the development of equatorial Pacific SSTA during boreal autumn and winter. According to North et al. (1982), this EOF mode is well separated from the remaining EOF modes. It seems that the impact of preceding SLPA on the succeeding El Niño events may depend not only on the intensity of the SLPA, but also on its spatial distribution. In spite of the small variance explained by the fourth EOF mode, its spatial pattern (Fig. 2) is significantly correlated with that of the SLPA associated with El Niño occurrence (Fig. 1) in boreal spring, with the spatial correlation coefficient as high as 0.43. Therefore, the sum of the first and fourth EOF modes in boreal spring exhibits a much greater contribution to the occurrence of succeeding El Niño events. It should be
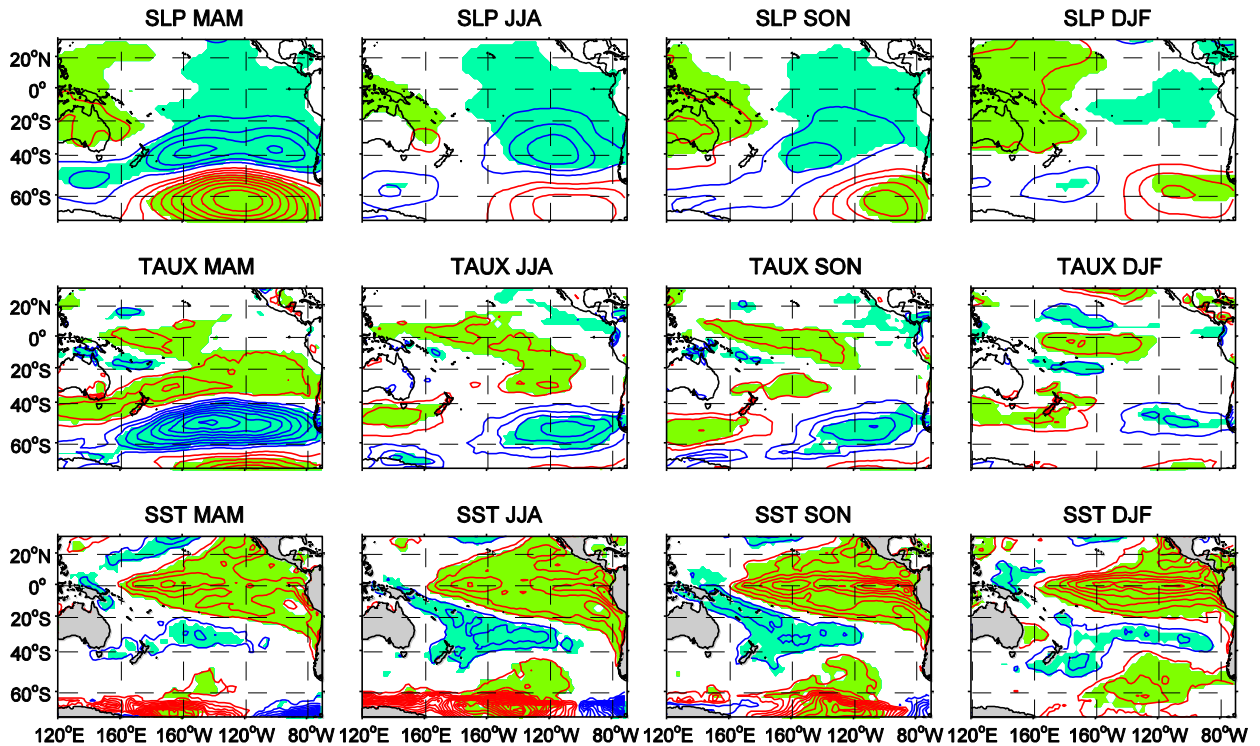
FIG. 5. As in Fig. 4, but against the sum of PCs of the first and fourth EOF modes.

noted that very strong SST anomalies appear around the Antarctic polar region in both Figs. 4 and 5. These large SST anomalies may not be true. They may be caused by the data error around the Antarctic polar region.

We further perform the mixed layer heat budget analysis in the equatorial eastern Pacific region (130°–80°W) to investigate the physical mechanisms responsible for the influence of the precursors outside the equatorial Pacific on the development of the equatorial eastern Pacific SSTA. Here we use the sum of PC1 and PC4 to regress each term in Eq. (1). The results are displayed in Fig. 6. In boreal autumn of El Niño years, there is a significant SST warming (Fig. 6a) in the equatorial Pacific, which is consistent with the results of regression analysis (Fig. 5). The surface heat flux mainly plays a role inhibiting the increase of mixed layer temperature (Fig. 6b). Among the advection terms, the contributions of $-\overline{w}dT'/dz$ (Fig. 6c), $-u'd\overline{T}/dx$ (Fig. 6d), $-v'd\overline{T}/dy$ (Fig. 6e), and $-\overline{v}dT'/dy$ (Fig. 6f) to the variation of SST tendency are relatively significant. Our results are same as those revealed by Zhu and Kumar (2018) that the zonal advective feedback ($-u'd\overline{T}/dx$, $-v'd\overline{T}/dy$), the mean current effect ($-\overline{v}dT'/dy$), and the thermocline feedback ($-\overline{w}dT'/dz$) are most important factors affecting El Niño evolution. As seen in Fig. 5, the anomalous westerly winds along the equator cause the anomalous eastward currents near the equatorial Pacific ($u' > 0$) and

an oceanic convergence ($v' < 0$ and $v' > 0$ to the north and south of the equator respectively). Considering the climatological SST distribution around the eastern equatorial Pacific ($d\overline{T}/dx < 0$; $d\overline{T}/dy > 0$ and $d\overline{T}/dy < 0$ to the north and south of equator, respectively), therefore both the contributions of $-u'd\overline{T}/dx$ and $-v'd\overline{T}/dy$ are positive, which increases the SST in the equatorial eastern Pacific. Therefore, the advection of climatological temperature by the anomalous ocean currents contributes to the occurrence of El Niño events. Moreover, near the eastern equatorial region in the South Pacific, the SSTA increases toward the equator ($dT'/dy > 0$) and climatological southward currents prevail ($\overline{v} < 0$), which make the term $-\overline{v}dT'/dy > 0$, indicating the advection of anomalous temperature by the climatological meridional current is also an important factor for the persistence of the positive SSTA in the eastern equatorial Pacific in boreal autumn and winter. Ding et al. (2015) reported that the South Pacific extratropical influence on ENSO involves the propagating process of subsurface temperature anomalies along the equator. The downwelling Kelvin wave excited by the anomalous westerly winds near the equator leads to a positive thermocline feedback.

b. Origin of the boreal spring South Pacific precursor

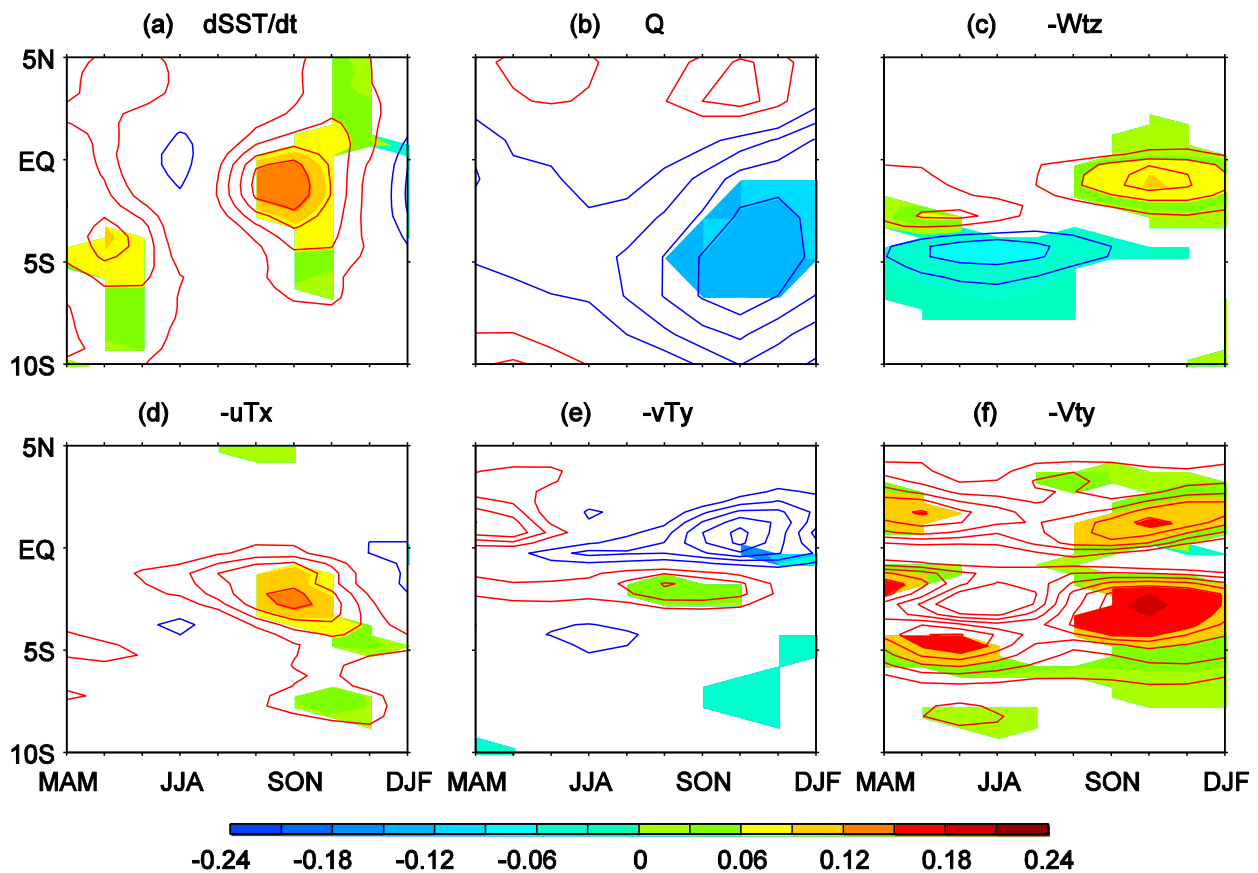Another important question to ask is what the origin is of the first and the fourth EOF modes of South Pacific

FIG. 6. Regressed (a) SST tendency, (b) the sum of surface heat flux terms, (c) $-\overline{w}dT'/dz$, (d) $-u'd\overline{T}/dx$, (e) $-v'd\overline{T}/dy$, and (f) $-\overline{v}dT'/dy$ against the sum of PCs of the first and fourth EOF modes for the MAM normalized SLPA field over South Pacific in the region 15°–75°S, 160°E–70°W. The heat budget is the average over the longitudes 130°–80°W. Contour intervals are 0.03°C month^{-1} °C^{-1}. The shaded areas are significant abve the 95% confidence level.

SLPA in boreal spring. Here we examine the EOFs of the 500-hPa geopotential height anomaly field in the Southern Hemisphere for the whole year (Fig. 7). The first mode is the southern annular mode (SAM), and the second and third modes represent the two modes of PSA pattern (i.e., PSA1 and PSA2, respectively) (Mo and Higgins 1998). However, the fourth EOF mode is well separated from the remaining EOF modes according to the criterion proposed by North et al. (1982), and has not been mentioned in previous studies possibly because of its relatively small explained variance. Here we defined it as PSA3.

We use the principal component time series of each EOF mode for the 500-hPa geopotential height field in the Southern Hemisphere to characterize the evolution of each mode. The simultaneous correlation coefficients between PC1 and PC4 of SLPA EOF modes shown in Fig. 3 and the PCs of EOF modes for South Hemisphere 500-hPa geopotential height anomaly in boreal spring are shown in Table 1. It can be seen that the first and

fourth EOF modes of SLPA in the 15°–75°S, 160°E–70°W region have the largest correlation coefficients, 0.84 and 0.64, with PSA1 and PSA3, respectively. We further calculated the lead–lag correlations of the first and fourth EOF modes of SLPA in the 15°–75°S, 160°E–70°W region with PSA1 and PSA3, respectively, and the results are shown in Fig. 8. It is obvious that PSA1 (Fig. 8a) and PSA3 (Fig. 8b) have a significant leading and lagging correlations with the first and fourth EOF modes of SLPA, respectively, but the highest correlation occurs simultaneously. That is to say, the SLPA signal associated with the SPO in boreal spring may be closely related to PSA1 and PSA3 in the Southern Hemisphere.

Considering the important role played by the SPO in the formation of the SPMM (You and Furtado 2018) and the influence of the SPMM on the SSTA in the eastern equatorial Pacific (Zhang et al. 2014; Min et al. 2017), we further investigate the relationship between the first/fourth EOF modes of SLPA in the 15°–75°S,
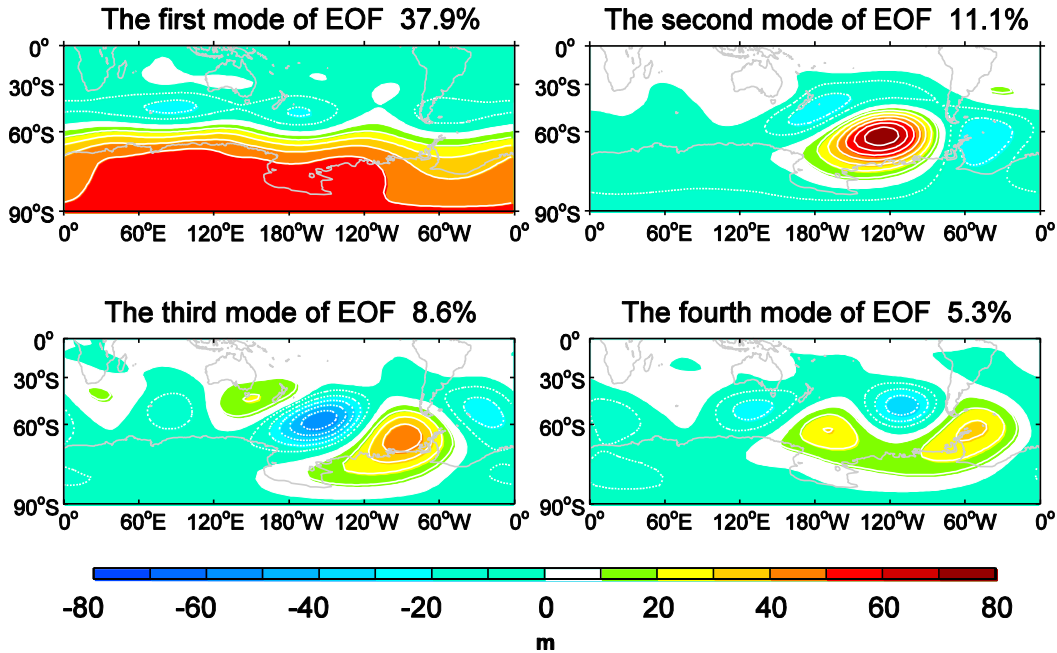
FIG. 7. The first four EOF modes of 500-hPa geopotential height anomaly in the Southern Hemisphere for the whole year. The solid and dashed lines indicate positive and negative anomalies, respectively.

160°E–70°W region and the SPMM. The lead–lag correlation coefficients between the PCs of the first/fourth EOF modes of SLPA and the SPMM index show that the first mode has no significant correlation with the SPMM in Sothern Hemisphere (Fig. 9a), but the fourth mode is significantly correlated with SPMM, with a simultaneous correlation coefficient of 0.74 (Fig. 9b). That is to say, only part of the boreal spring SLPA (PSA3) associated with the SPO can exert a significant impact on the development of the SPMM, and the impact of the SPMM on the SSTA in eastern equatorial Pacific seems to occur only through the part of PSA3. Here we demonstrated that the PSA3, revealed in this study, may be an important anomalous atmospheric circulation pattern in the formation of the SPMM, in addition to its impact on El Niño events.

TABLE 1. Simultaneous correlation coefficients between the PC1 (PC4) of the first (fourth) EOF modes for SLPA over 15°–75°S, 160°E–70°W and the PCs for the Southern Hemisphere 500-hPa geopotential height anomaly in boreal spring. An asterisk (*) indicates that the correlation coefficient exceeds the 95% significant level.

	SLPA PC1	SLPA PC4
SH Z_{500} PC1	0.45*	−0.50*
SH Z_{500} PC2	0.84*	0.22
SH Z_{500} PC3	−0.34*	0.10
SH Z_{500} PC4	−0.05	0.64*

c. A simple statistical model for predicting eastern equatorial Pacific SSTA in boreal winter

In the previous sections, we have presented evidence of the relationship between the South Pacific SLPA in boreal spring of El Niño years and the evolution of El Niño. However, can the South Pacific SLPA in boreal spring be used as a reasonable precursor to predict the development of SSTA in equatorial Pacific? We now put these findings to the test in a simple predictive exercise to check its ability in long-lead El Niño prediction. Here, we try to construct a simple statistical model, and introduce the South Pacific SLPA in boreal spring as a precursor and compare the prediction skill predicted by the SPMM in the same period. We construct the simple multivariate statistical models in the following forms:

$$SSTA_{DJF}(x, t) = a(x) \times SLPA_{PC1_{MAM(t)}} + b(x) \times SLPA_{PC4_{MAM(t)}} + \varepsilon, \quad (2)$$

$$SSTA_{DJF}(x, t) = c(x) \times SPMM_{MAM(t)} + \varepsilon, \quad (3)$$

where x is the spatial coordinate, t is time, and a, b, and c are the regression coefficients determined by least squares fitting; $SLPA_{PC1_{MAM(t)}}$ and $SLPA_{PC4_{MAM(t)}}$ are the principal component time series of the first and the fourth mode of SLPA in the 15°–75°S, 160°E–70°W region during boreal spring, respectively; and $SPMM_{MAM(t)}$ is the boreal spring
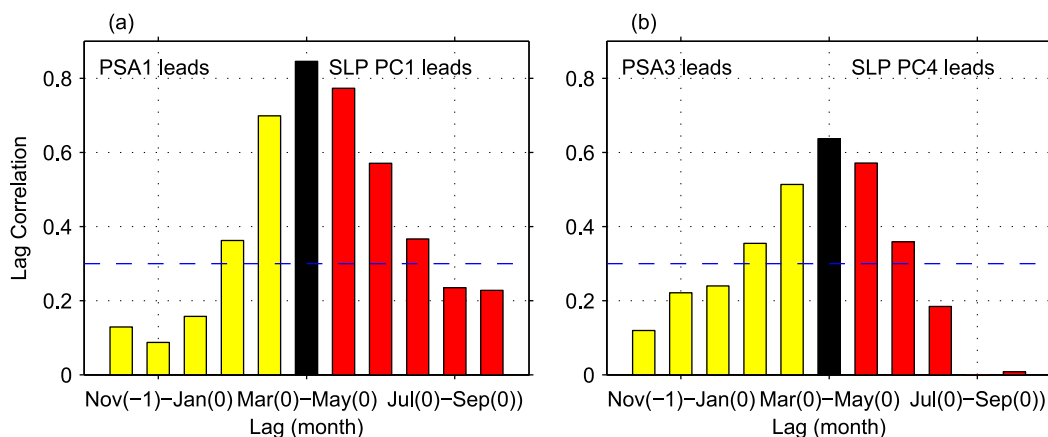
FIG. 8. Lead–lag correlation coefficients of (a) PSA1 and (b) PSA3 with the PCs of the first and fourth EOF modes, respectively, for the MAM normalized SLPA field over South Pacific in the region 15°–75°S, 160°E–70°W. The black bar shows simultaneous correlations, and yellow (red) shaded bars represent PSA leading (lagging) the PCs. The dashed lines indicate significance at the 99% confidence level. The PSA1 and PSA3 are obtained by performing the EOF analysis separately on different seasons and then the lead–lag correlation with MAM SLPA is calculated.

SPMM index. To score the skill of this simple model in predicting El Niño intensity and related SSTA distribution, the target variable is set as the SSTA over the Pacific basin in boreal winter (December–February). The anomaly correlation coefficient (ACC; Miyakoda et al.1972) is used to quantify the forecast skills of the statistical models. The ACC can be expressed as

$$\mathrm{ACC} = \frac{\sum\limits_{t=1}^{T} f_t v_t}{\sqrt{\sum\limits_{t=1}^{T} f_t^2}\sqrt{\sum\limits_{t=1}^{T} v_t^2}}, \qquad (4)$$

where f_t is the forecast value and v_t is the observed value at time t. The leave-one-out cross-validation scheme is applied to reduce overfitting (Elsner and Schmertmann 1994).

The performance of the statistical models is summarized in Fig. 10. When using the South Pacific (15°–75°S, 160°E–70°W) SLPA in boreal spring as a precursor, high ACC values prevail in the tropical eastern and central Pacific (Fig. 10a). The ACC values of the eastern equatorial Pacific to the east of the date line are generally higher than 0.4, and the ACC values in the eastern and southeastern equatorial Pacific region are higher than 0.5. If we only use SPMM$_{\mathrm{MAM}(t)}$ as precursor, all the ACC values near the equator are lower than 0.4
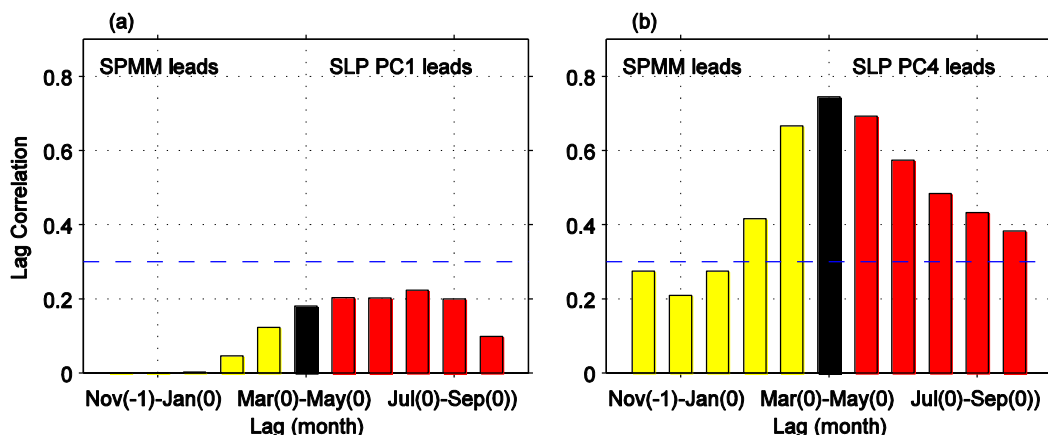

FIG. 9. As in Fig. 8, but for correlation coefficients of SPMM with the PCs of the (a) first and (b) fourth EOF modes. Yellow (red) shaded bars represent SPMM leading (lagging) the PCs. The SPMM-wind indices on different seasons are obtained by performing MCA analysis on corresponding seasons, and then the lead–lag correlation with MAM SLPA is calculated.
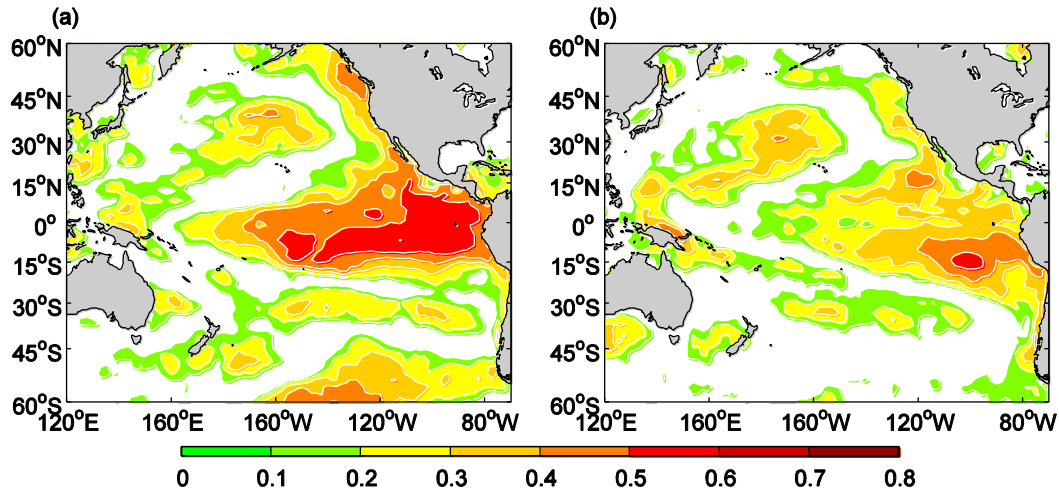
FIG. 10. ACC of $SSTA_{DJF}$ predicted by simple linear regression models in considering (a) both the South Pacific SLPA_PC1$_{MAM}$ and SLPA_PC4$_{MAM}$, and (b) the SPMM$_{MAM}$. The shaded areas are significant above the 95% confidence level per a Monte Carlo test.

(Fig. 10b). Compared to Fig. 10a, ACC values higher than 0.4 in Fig. 10b only appear in a much smaller area of the eastern equatorial Pacific. Such results indicate that the precursor of South Pacific SLPA in boreal spring has the ability to predict the evolution of SSTA in eastern equatorial Pacific, and its prediction skill is better than that of SPMM during the same period. It is also further demonstrated that the SLPA founded in our present study plays a more important role in El Niño occurrence than the SPMM. In fact, a recent study by Ding et al. (2020) also revealed that, compared to other South Pacific precursors, the SPMM may not be a reliable precursor for ENSO.

4. Summary and discussion

The composites of SLPA field in El Niño years indicate that in South Pacific there are two significant negative SLPA centers at around 40°S, 165°W and 40°S, 110°W in the north and one significant positive SLPA center at around 65°S, 140°W in the south during boreal spring of El Niño years. It is found that this SLPA pattern is essentially a precursory signal of SPO in boreal spring. The SPO signal is strongest in boreal summer, effectively weakens the intensity of trade winds near equatorial Pacific, and further promotes the warming of SST in the eastern equatorial Pacific, which is conducive to the development of El Niño events. You and Furtado (2017) pointed out that the strong SPO signals in boreal summer may provide a reasonable index for the prediction of the development of specific types of El Niño, which can better predict the type of El Niño in 6 months before El Niño reaches its peak. However, results in this

study indicate that the early sign of SLPA in boreal spring may be a good precursor for the occurrence of El Niño events. In addition, we find that the fourth EOF mode of the 500-hPa geopotential height anomaly field in the Southern Hemisphere in boreal spring of El Niño years, named as PSA3 in our present study, has an important influence on the evolution of the SPO and the development of SPMM in the southeastern Pacific. It is revealed that the SLPA in boreal spring of El Niño years related to the SPO is not a single EOF mode, but the result of an interaction of two independent EOF modes of PSA1 and PSA3 in the same period. The variation of SPMM in boreal spring is only highly correlated with the part of PSA3 that is related with the SPO in the southeastern Pacific. However, both the two independent modes of PSA1 and PSA3 contribute to the development of SSTA in the equatorial eastern Pacific. This may provide a physical explanation as to why the prediction skill with the boreal spring SLPA as a precursor is better to some extent in predicting El Niño occurrence than that with the boreal spring SPMM.

This study investigates and discusses the significance of the South Pacific SLPA during boreal spring as a precursor for the evolution of SSTA in eastern equatorial Pacific, and emphasizes the contribution of the South Pacific atmospheric variability to El Niño occurrence. Many studies have proposed the importance of precursor signals over the Northern Hemisphere, such as NPO and NPMM, in El Niño occurrence. Ding et al. (2019) proposed that North and South Pacific SST precursors make comparable contributions to ENSO. However, as seen in Fig. 1, the signals of precursor SLPA are very weak prior to El Niño occurrence from early

boreal spring to summer in the Northern Hemisphere. The relative importance of the signals from the Northern and Southern Hemispheres in El Niño occurrence is an interesting topic for further investigation. Meanwhile, in this study the anomalous features of SLPA as well as the atmospheric circulations in middle troposphere during boreal spring prior to El Niño occurrence are revealed. However, it is still not clear how these anomalies are formed, and especially what the physical meanings are of the PSA3 we introduced. Further research is needed for solving such issues. Additionally, in this study we focused on conventional El Niño events. How the precursor signals revealed in our present study impact central Pacific and eastern Pacific El Niños is worthy of further investigation.

REFERENCES

Alexander, M. A., D. J. Vimont, P. Chang, and J. D. Scott, 2010: The impact of extratropical atmospheric variability on ENSO: Testing the seasonal footprinting mechanism using coupled model experiments. *J. Climate*, **23**, 2885–2901, https://doi.org/10.1175/2010JCLI3205.1.

Anderson, B. T., and R. C. Perez, 2015: ENSO and non-ENSO induced charging and discharging of the equatorial Pacific. *Climate Dyn.*, **45**, 2309–2327, https://doi.org/10.1007/s00382-015-2472-x.

——, ——, and A. Karspeck, 2013: Triggering of El Niño onset through trade wind-induced charging of the equatorial Pacific. *Geophys. Res. Lett.*, **40**, 1212–1216, https://doi.org/10.1002/grl.50200.

Ashok, K., S. K. Behera, S. A. Rao, H. Weng, and T. Yamagata, 2007: El Niño Modoki and its possible teleconnection. *J. Geophys. Res.*, **112**, C11007, https://doi.org/10.1029/2006JC003798.

Bretherton, C. S., C. Smith, and J. M. Wallace, 1992: An intercomparison of methods for finding coupled patterns in climate data. *J. Climate*, **5**, 541–560, https://doi.org/10.1175/1520-0442(1992)005<0541:AIOMFF>2.0.CO;2.

Carton, J. A., and B. S. Giese, 2008: A reanalysis of ocean climate using Simple Ocean Data Assimilation (SODA). *Mon. Wea. Rev.*, **136**, 2999–3017, https://doi.org/10.1175/2007MWR1978.1.

Chang, P., L. Zhang, R. Saravanan, D. J. Vimont, J. C. H. Chiang, L. Ji, H. Seidel, and M. K. Tippett, 2007: Pacific meridional mode and El Niño–Southern Oscillation. *Geophys. Res. Lett.*, **34**, L16608, https://doi.org/10.1029/2007GL030302.

Chiang, J. C. H., and D. J. Vimont, 2004: Analogous Pacific and Atlantic meridional modes of tropical atmosphere–ocean variability. *J. Climate*, **17**, 4143–4158, https://doi.org/10.1175/JCLI4953.1.

de Boyer Montégut, C., G. Madec, A. S. Fischer, A. Lazar, and D. Iudicone, 2004: Mixed layer depth over the global ocean: An examination of profile data and a profile-base

climatology. *J. Geophys. Res.*, **109**, C12003, https://doi.org/10.1029/2004JC002378.

Deser, C., and J. M. Wallace, 1990: Large-scale atmospheric circulation features of warm and cold episodes in the tropical Pacific. *J. Climate*, **3**, 1254–1281, https://doi.org/10.1175/1520-0442(1990)003<1254:LSACFO>2.0.CO;2.

Di Lorenzo, E., G. Liguori, N. Schneider, J. C. Furtado, B. T. Anderson, and M. A. Alexander, 2015: ENSO and meridional modes: A null hypothesis for Pacific climate variability. *Geophys. Res. Lett.*, **42**, 9440–9448, https://doi.org/10.1002/2015GL066281.

Ding, R. Q., J. P. Li, and Y.-H. Tseng, 2015: The impact of South Pacific extratropical forcing on ENSO and comparisons with the North Pacific. *Climate Dyn.*, **44**, 2017–2034, https://doi.org/10.1007/s00382-014-2303-5.

——, ——, Y. H. Tseng, C. Sun, and F. Zheng, 2017a: Linking a sea level pressure anomaly dipole over North America to the central Pacific El Niño. *Climate Dyn.*, **49**, 1321–1339, https://doi.org/10.1007/s00382-016-3389-8.

——, J. Li, Y.-H. Tseng, C. Sun, and F. Xie, 2017b: Joint impact of North and South Pacific extratropical atmospheric variability on the onset of ENSO events. *J. Geophys. Res. Atmos.*, **122**, 279–298, https://doi.org/10.1002/2016JD025502.

——, Y.-H. Tseng, J. P. Li, C. Sun, F. Xie, and Z. Hou, 2019: Relative contributions of North and South Pacific sea surface temperature anomalies to ENSO. *J. Geophys. Res.*, **124**, 6222–6237, https://doi.org/10.1029/2018JD030181.

——, J. Li, R. Yang, Y. Tseng, Y. Li, and K. Ji, 2020: On the differences between the South Pacific meridional and quadrupole modes. *J. Geophys. Res. Oceans*, **125**, e2019JC015500, https://doi.org/10.1029/2019JC015500.

Elsner, J. B., and C. P. Schmertmann, 1994: Assessing forecast skill through cross validation. *Wea. Forecasting*, **9**, 619–624, https://doi.org/10.1175/1520-0434(1994)009<0619:AFSTCV>2.0.CO;2.

Fedorov, A. V., 2002: The response of the coupled tropical ocean–atmosphere to westerly wind bursts. *Quart. J. Roy. Meteor. Soc.*, **128**, 1–23, https://doi.org/10.1002/qj.200212857901.

Kalnay, E., and Coauthors, 1996: The NCEP/NCAR 40-Year Reanalysis Project. *Bull. Amer. Meteor. Soc.*, **77**, 437–471, https://doi.org/10.1175/1520-0477(1996)077<0437:TNYRP>2.0.CO;2.

Kao, H.-Y., and J.-Y. Yu, 2009: Contrasting eastern Pacific and central Pacific types of El Niño. *J. Climate*, **22**, 615–632, https://doi.org/10.1175/2008JCLI2309.1.

Kug, J.-S., F.-F. Jin, and S.-I. An, 2009: Two types of El Niño events: Cold tongue El Niño and warm pool El Niño. *J. Climate*, **22**, 1499–1515, https://doi.org/10.1175/2008JCLI2624.1.

Larson, S. M., and B. P. Kirtman, 2014: The Pacific meridional mode as an ENSO precursor and predictor in the North American Multimodel Ensemble. *J. Climate*, **27**, 7018–7032, https://doi.org/10.1175/JCLI-D-14-00055.1.

Linkin, M. E., and S. Nigam, 2008: The North Pacific Oscillation–west Pacific teleconnection pattern: Mature-phase structure and winter impacts. *J. Climate*, **21**, 1979–1997, https://doi.org/10.1175/2007JCLI2048.1.

McGregor, S., N. J. Holbrook, and S. B. Power, 2009a: The response of a stochastically forced ENSO model to observed off-equatorial wind-stress forcing. *J. Climate*, **22**, 2512–2525, https://doi.org/10.1175/2008JCLI2387.1.

——, A. Sen Gupta, N. J. Holbrook, and S. B. Power, 2009b: The modulation of ENSO variability in CCSM3 by extratropical Rossby waves. *J. Climate*, **22**, 5839–5853, https://doi.org/10.1175/2009JCLI2922.1.

McPhaden, M. J., 2012: A 21st century shift in the relationship between ENSO SST and warm water volume anomalies. *Geophys. Res. Lett.*, **39**, L09706, https://doi.org/10.1029/2012GL051826.

Meinen, C. S., and M. J. McPhaden, 2000: Observations of warm water volume changes in the equatorial Pacific and their relationship to El Niño and La Niña. *J. Climate*, **13**, 3551–3559, https://doi.org/10.1175/1520-0442(2000)013<3551:OOWWVC>2.0.CO;2.

Min, Q., J. Su, R. Zhang, and X. Rong, 2015: What hindered the El Niño pattern in 2014? *Geophys. Res. Lett.*, **42**, 6762–6770, https://doi.org/10.1002/2015GL064899.

——, ——, and ——, 2017: Impact of the South and North Pacific meridional modes on the El Niño–Southern Oscillation: Observational analysis and comparison. *J. Climate*, **30**, 1705–1720, https://doi.org/10.1175/JCLI-D-16-0063.1.

Miyakoda, K., G. D. Hembree, R. F. Strickler, and I. Shulman, 1972: Cumulative results of extended forecast experiments I. Model performance for winter cases. *Mon. Wea. Rev.*, **100**, 836–855, https://doi.org/10.1175/1520-0493(1972)100<0836:CROEFE>2.3.CO;2.

Mo, K. C., and R. W. Higgins, 1998: The Pacific–South American modes and tropical convection during the Southern Hemisphere winter. *Mon. Wea. Rev.*, **126**, 1581–1596, https://doi.org/10.1175/1520-0493(1998)126<1581:TPSAMA>2.0.CO;2.

North, G. R., T. L. Bell, and R. F. Cahalan, 1982: Sampling errors in the estimation of empirical orthogonal functions. *Mon. Wea. Rev.*, **110**, 699–706, https://doi.org/10.1175/1520-0493(1982)110<0699.

Pierce, D. W., T. P. Barnett, and M. Latif, 2000: Connections between the Pacific Ocean tropics and midlatitudes on decadal timescales. *J. Climate*, **13**, 1173–1194, https://doi.org/10.1175/1520-0442(2000)013<1173:CBTPOT>2.0.CO;2.

Poli, P., and Coauthors, 2013: The data assimilation system and initial performance evaluation of the ECMWF pilot reanalysis of the 20th-century assimilating surface observations only (ERA-20C). ERA Rep. Series, Rep. 14, 59 pp., http://www.ecmwf.int/en/elibrary/11699-data-assimilation-system-andinitial-performance-evaluation-ecmwf-pilot-reanalysis.

Rogers, J. C., 1981: The North Pacific Oscillation. *Int. J. Climatol.*, **1**, 39–57, https://doi.org/10.1002/joc.3370010106.

Saha, S., and Coauthors, 2006: The NCEP Climate Forecast System. *J. Climate*, **19**, 3483–3517, https://doi.org/10.1175/JCLI3812.1.

Su, J., R. Zhang, X. Rong, Q. Min, and C. Zhu, 2018: Sea surface temperature in the subtropical Pacific boosted the 2015 El Niño and hindered the 2016 La Niña. *J. Climate*, **31**, 877–893, https://doi.org/10.1175/JCLI-D-17-0379.1.

Sun, D.-Z., T. Zhang, and S.-I. Shin, 2004: The effect of subtropical cooling on the amplitude of ENSO: A numerical study. *J. Climate*, **17**, 3786–3798, https://doi.org/10.1175/1520-0442(2004)017<3786:TEOSCO>2.0.CO;2.

Trenberth, K. E., and D. P. Stepaniak, 2001: Indices of El Niño evolution. *J. Climate*, **14**, 1697–1701, https://doi.org/10.1175/1520-0442(2001)014<1697:LIOENO>2.0.CO;2.

Vimont, D. J., D. S. Battisti, and A. C. Hirst, 2001: Footprinting: A seasonal connection between the tropics and mid-latitudes. *Geophys. Res. Lett.*, **28**, 3923–3926, https://doi.org/10.1029/2001GL013435.

——, ——, and ——, 2003a: The seasonal footprinting mechanism in the CSIRO general circulation models. *J. Climate*, **16**, 2653–2667, https://doi.org/10.1175/1520-0442(2003)016<2653:TSFMIT>2.0.CO;2.

——, J. M. Wallace, and D. S. Battisti, 2003b: The seasonal footprinting mechanism in the Pacific: Implications for ENSO. *J. Climate*, **16**, 2668–2675, https://doi.org/10.1175/1520-0442(2003)016<2668:TSFMIT>2.0.CO;2.

——, ——, and M. Newman, 2014: Optimal growth of central and East Pacific ENSO events. *Geophys. Res. Lett.*, **41**, 4027–4034, https://doi.org/10.1002/2014GL059997.

Walker, G., and E. Bliss, 1932: World weather V. *Mem. Roy. Meteor. Soc.*, **4**, 53–84.

Wang, C. Z., and R. H. Weisberg, 2000: The 1997–98 El Niño evolution relative to previous El Niño events. *J. Climate*, **13**, 488–501, https://doi.org/10.1175/1520-0442(2000)013<0488:TENOER>2.0.CO;2.

Xie, S.-P., and S. G. H. Philander, 1994: A coupled ocean–atmosphere model of relevance to the ITCZ in the eastern Pacific. *Tellus*, **46A**, 340–350, https://doi.org/10.3402/tellusa.v46i4.15484.

You, Y., and J. C. Furtado, 2017: The role of South Pacific atmospheric variability in the development of different types of ENSO. *Geophys. Res. Lett.*, **44**, 7438–7446, https://doi.org/10.1002/2017GL073475.

——, and ——, 2018: The South Pacific meridional mode and its role in tropical Pacific climate variability. *J. Climate*, **31**, 10 141–10 163, https://doi.org/10.1175/JCLI-D-17-0860.1.

——, and ——, 2019: The relationship between South Pacific atmospheric internal variability and ENSO in the North American Multimodel Ensemble Phase-II models. *Geophys. Res. Lett.*, **46**, 12 398–12 407, https://doi.org/10.1029/2019GL084637.

Yu, J.-Y., and S. T. Kim, 2011: Relationships between extratropical sea level pressure variations and the central Pacific and eastern Pacific types of ENSO. *J. Climate*, **24**, 708–720, https://doi.org/10.1175/2010JCLI3688.1.

——, H.-Y. Kao, and T. Lee, 2010: Subtropics-related interannual sea surface temperature variability in the equatorial central Pacific. *J. Climate*, **23**, 2869–2884, https://doi.org/10.1175/2010JCLI3171.1.

Zhang, H., A. Clement, and P. Di Nezio, 2014: The South Pacific meridional mode: A mechanism for ENSO-like variability. *J. Climate*, **27**, 769–783, https://doi.org/10.1175/JCLI-D-13-00082.1.

Zhang, R., and G. Zhao, 2001: Meridional wind stress anomalies over tropical pacific and the onset of El Niño. Part II: Dynamical analysis. *Adv. Atmos. Sci.*, **18**, 1053–1065, https://doi.org/10.1007/s00376-001-0022-4.

——, ——, and Y. Tan, 2001: Meridional wind stress anomalies over tropical Pacific and the onset of El Niño. Part I: Data analysis. *Adv. Atmos. Sci.*, **18**, 467–480, https://doi.org/10.1007/s00376-001-0038-9.

Zheng, Y., R. Zhang, and M. A. Bourassa, 2014: Impact of East Asian winter and Australian summer monsoons on the enhanced surface westerlies over the western tropical Pacific Ocean preceding the El Niño onset. *J. Climate*, **27**, 1928–1944, https://doi.org/10.1175/JCLI-D-13-00369.1.

Zhu, J., and A. Kumar, 2018: Influence of surface nudging on climatological mean and ENSO feedbacks in a coupled model. *Climate Dyn.*, **50**, 571–586, https://doi.org/10.1007/s00382-017-3627-8.

——, B. Huang, and M. A. Balmaseda, 2012: An ensemble estimation of the variability of upper-ocean heat content over the tropical Atlantic Ocean with multi-ocean reanalysis products. *Climate Dyn.*, **39**, 1001–1020, https://doi.org/10.1007/s00382-011-1189-8.